

PHASE-CONTROLLED INVERTERS ASSOCIATED TO A MULTI-PULSE AUTOTRANSFORMER APPLIED TO PHOTOVOLTAIC COGENERATION

Lucas Lapolli Brighenti, Luís G. Kremer, Alessandro L. Batschauer and Marcello Mezaroba.

Electric Power Processing Group – nPEE
 Santa Catarina State University - UDESC – CCT – DEE
 Campus Universitário, s/n, PO BOX 89223-100, Joinville, SC, Brazil
www.npee.joinville.udesc.br – lucasbrighenti@msn.com

Abstract – This paper presents the study of phase-controlled inverters associated to an 18-pulse autotransformer with Y-differential connection for photovoltaic energy cogeneration. The main objective of this system is to perform the cogeneration of photovoltaic energy on a simple, robust and cheaper way, aiming the application on remote places, which presents more rigorous climate conditions and where the size and volume are not a relevant factor. With the differential configuration, the autotransformer processes just 22% of the total power provided to the system by the photovoltaic panels, reducing significantly the overall cost. On other hand, the 18-pulses connection allows low THD quasi-sinusoidal output currents, minimizing the needed of output filters. This proposed system is composed by simple and well known technologies that use phase-controlled inverters and autotransformer, so it can be a robust, simple and low-cost solution for photovoltaic cogeneration.

Keywords – autotransformer, phase-controlled inverters, photovoltaic cogeneration, SCR, Y-differential connection.

I - INTRODUCTION

Electrical energy obtained from photovoltaic panels needs to be processed before being matched to the distribution system.

This work proposes a robust system to process energy provided by photovoltaic panels, with easy maintenance, low THD and high power factor, to be installed at secluded places, where reliability and cost are important facts to be considered, while weight and volume are not the most relevant aspects. This project uses phase-controlled inverters, a consolidated technology that offers a robust, low-cost solution to convert energy provided by the panels and inject it at the grid.

The complete system is composed by three photovoltaic arrays connected to a DC-DC converter to produce the MPPT and adapt the voltage to the required levels of the inverters, which are associated to an 18-pulse autotransformer, as shown at Fig. 1.

The focus of this work is restricted at the grid inverter, as shown at Fig. 2. The photovoltaic panels and the DC-DC converters (responsible to make the MPPT) are represented as continuous current sources. The current injected by each non-autonomous phase-controlled inverter has a high total harmonic distortion (THD). Aiming to reduce those harmonic contents, this design proposes the use of an 18-pulse autotransformer with Y-differential connection, reducing the THD levels to meet the energy quality standards. This system has a dual circuit of the multi-pulse rectifiers, which are used to obtain rectified voltages with low ripple and a high power factor [2, 3].

This topology presents a theoretical power factor of 0.995 and a THD of 10.05%. Other great advantage of this topology are the differential connections, that limits the total power processed by the autotransformer in 21.88% of total power processed by the inverters, so the autotransformer's volume and weight can be substantially reduced and, due to it, the total cost of this converter becomes cheaper than the converters that use isolated transformers.

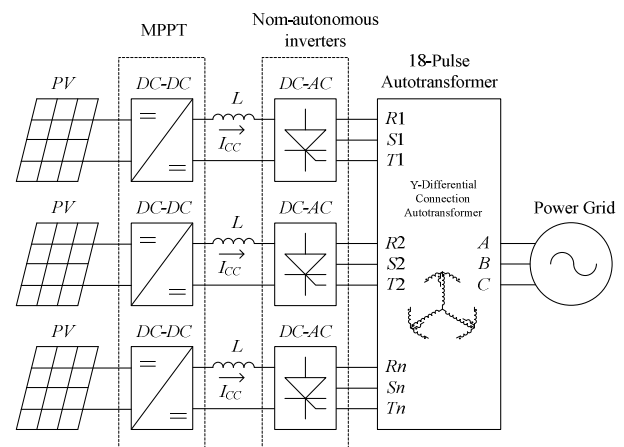


Fig. 1 – General scheme of the proposed system.

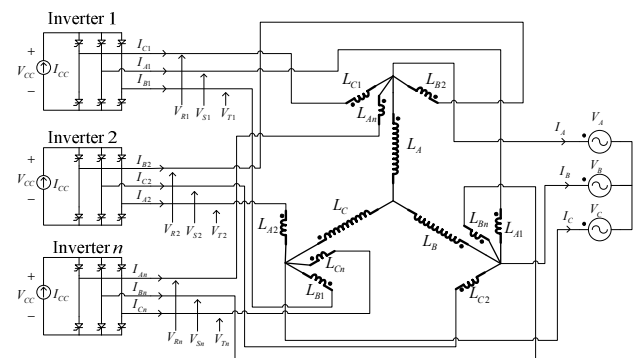


Fig. 2. Phase-controlled inverters associated to an 18-pulse autotransformer with closed Y-differential connection.

II - PHASE-CONTROLLED INVERTER

The non-autonomous phase-controlled inverter is a static converter, which makes the conversion of a continuous current to an alternate current and needs to be connected to the grid for its correct operation. This inverter is composed by a silicon controlled rectifier (SCR) Graetz bridge and a synchronized phase control circuit. In this application, the gate pulse is fixed in an angle of 180° , to ensure its operation as an inverter. The current injected in the grid by the inverter is shown in Fig. 3. Fig. 4 shows voltage and current at the DC side of the inverter.

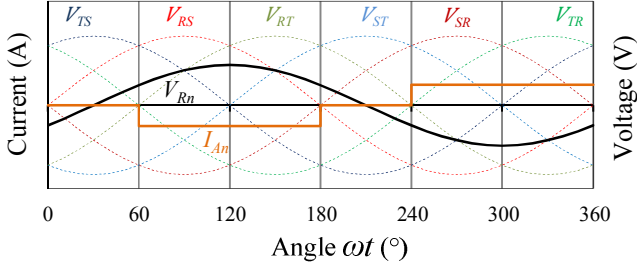


Fig. 3. Voltage and current injected in the grid by a single phase-controlled inverter.

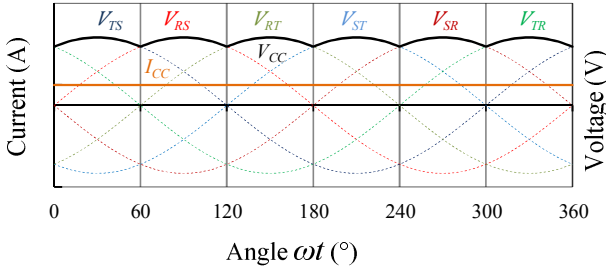


Fig. 4. Voltage and current drained from the photovoltaic panels (represented by a current source).

III - 18-PULSE AUTOTRANSFORMER

To obtain the 18-pulses grid current, it is necessary a 20° of displacement between the subsystems where the inverters are connected. The closed Y-differential connection was chosen because it presents a step-down voltage relative to the grid voltage, becoming an attractive choice for PV applications. The voltage shifts of 20° are created by combining the amplitude of the voltage vectors existing in autotransformer windings, as shown at Fig. 5.

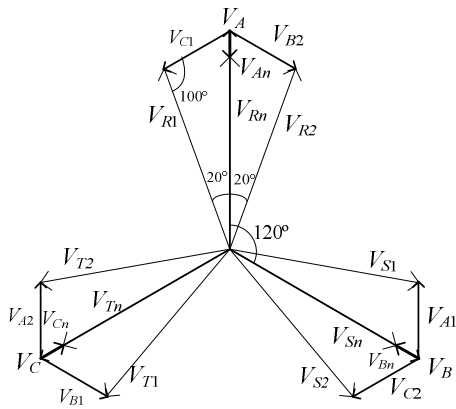


Fig. 5. Complete voltage vectors at the 18-pulse autotransformer.

The turn ratios for the secondary windings are obtained from the trigonometric relations:

$$V_{B2} = V_{C1} = V_A \frac{\sin(20^\circ)}{\sin(100^\circ)} = 0.3473V_A \quad (1)$$

$$V_{R2} = V_{R1} = V_{Rn} = \frac{\sin(60^\circ)}{\sin(100^\circ)} V_A = 0.8794V_A \quad (2)$$

$$V_{An} = V_A - V_{Rn} = V_A - 0.8794V_A = 0.1206V_A \quad (3)$$

$$N_{0^\circ} = \frac{V_A}{V_{An}} = \frac{V_A}{0.1206V_A} = 8.2819 \quad (4)$$

$$N_{20^\circ} = \frac{V_A}{V_{B2}} = \frac{V_A}{0.3473V_A} = 2.8794 \quad (5)$$

TABLE I
Turns and voltage ratio for phase A

| V_{A1}, V_{A2} | $0.3473V_A$ |
|--------------------------|-------------|
| V_{An} | $0.1206V_A$ |
| V_{R1}, V_{R2}, V_{Rn} | $0.8794V_A$ |
| N_{20° | 2.8794 |
| N_{0° | 8.2819 |

Fig. 6 presents the waveforms to voltages V_{R1} , V_{R2} , V_{Rn} and V_A :

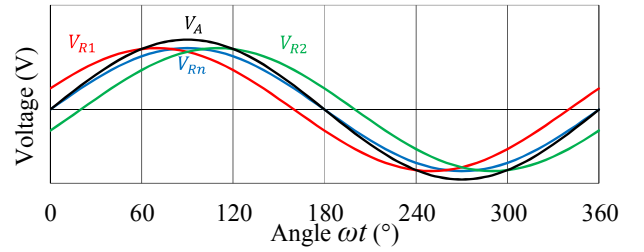


Fig. 6 - Voltages V_{R1} , V_A , V_{Rn} and V_{R2} showing the 20° shift among the voltages.

A. Current analysis

Fig. 7 shows the winding currents and the voltage vectors to each subsystem. It is important to notice that the three phases (R, S and T) of every subsystem feed one inverter, according to Fig. 2, and the currents are presented with the nomenclature of the winding where it passes, and not by the feeding voltage. Currents that enter in the secondary windings are injected by the inverters, as presented at Fig. 3.

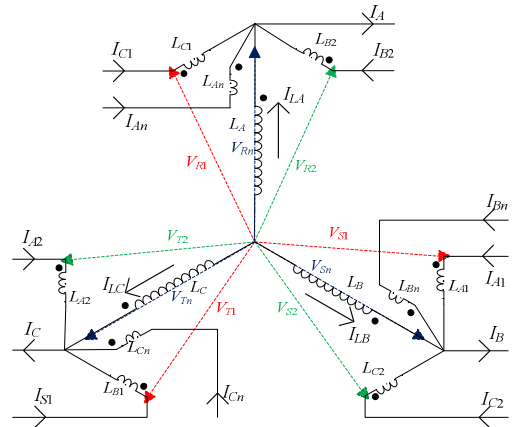


Fig. 7. Winding currents in autotransformer.

1) Currents at the primary windings (L_A , L_B and L_C) - Windings L_A , L_{A1} , L_{A2} and L_{An} are magnetically coupled, in

other words, they are at the same leg of the autotransformer core, as well as L_B , L_{B1} , L_{B2} , L_{Bn} and L_C , L_{C1} , L_{C2} , L_{Cn} . Currents at the primary are composed by currents at the secondary windings referred to the primary. They are given by the following equations:

$$i_{LA}(t) = [i_{A1}(t) + i_{A2}(t)]/N_{20^\circ} - i_{An}(t)/N_{0^\circ} \quad (6)$$

$$i_{LB}(t) = [i_{B1}(t) + i_{B2}(t)]/N_{20^\circ} - i_{Bn}(t)/N_{0^\circ} \quad (7)$$

$$i_{LC}(t) = [i_{C1}(t) + i_{C2}(t)]/N_{20^\circ} - i_{Cn}(t)/N_{0^\circ} \quad (8)$$

Fig. 8 shows the voltage at phase A and the current in the primary windings of the autotransformer.

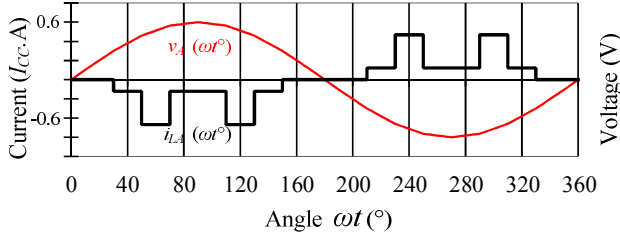


Fig. 8 – Voltage at phase A and current at the primary winding L_A .

Fig. 9 presents the graphic representation of the currents using (6). It could be observed that the current i_{LA} is a composition of the currents i_{A1} , i_{A2} and i_{An} .

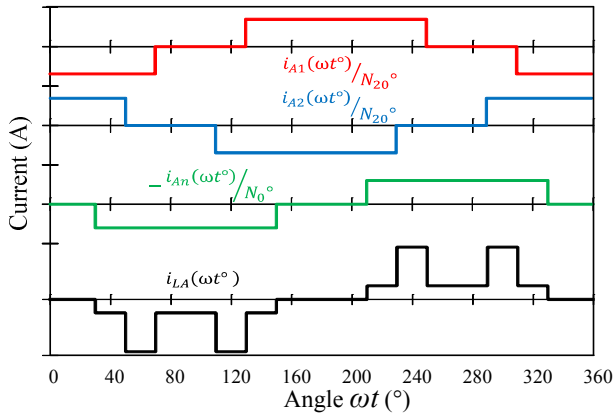


Fig. 9. Graphic generation of i_{LA} current.

2) Currents injected in the grid (I_A , I_B and I_C) - Fig. 7 shows a circuit that emphasizes the behavior of the currents I_A , I_B , I_C . They are composed by the addition of the currents of the primary and secondary windings, such as follow:

$$i_A(t) = i_{LA}(t) + i_{C1}(t) + i_{B2}(t) + i_{An}(t) \quad (9)$$

$$i_B(t) = i_{LB}(t) + i_{A1}(t) + i_{C2}(t) + i_{Bn}(t) \quad (10)$$

$$i_C(t) = i_{LC}(t) + i_{B1}(t) + i_{A2}(t) + i_{Cn}(t) \quad (11)$$

The grid current waveform i_A and the voltage at phase A are presented in Fig. 10.

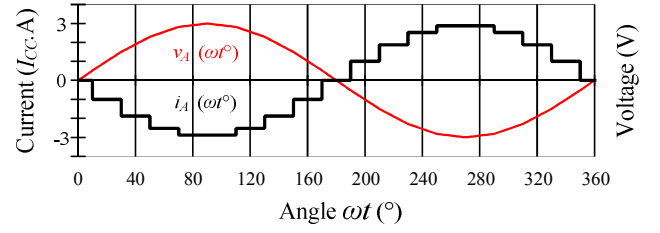


Fig. 10 – Input voltage and current at phase A.

Fig. 10 shows that the current injected at the grid presents an 18-pulse quasi-sinusoidal shape, which results on a low THD and a high power factor. Fig. 11 shows the graphic representation of the phase A current generation, according with (9), (10) and (11).

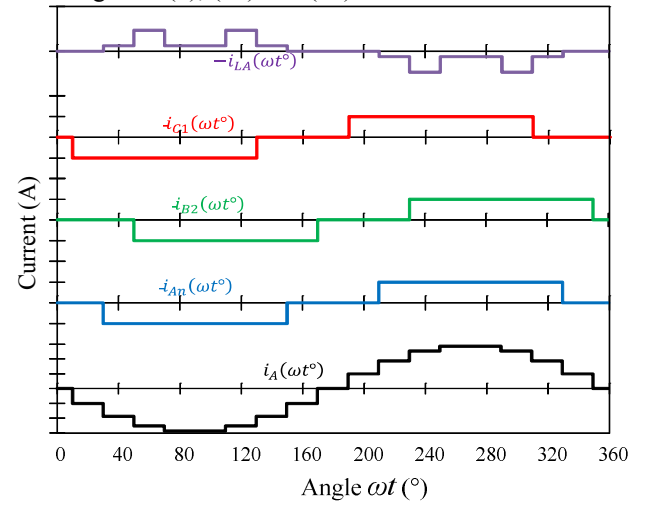


Fig. 11. Currents at the winding that compose the current injected at phase A.

IV - MATHEMATICAL ANALYSIS

A. Inverter Analysis

In the Graetz Bridge topology, the DC voltage is composed by the AC grid's line voltage:

$$V_{RnSn} = \sqrt{3}V_{Rn} = 0.8794\sqrt{3}V_A \quad (12)$$

$$V_{CC} = \frac{1}{T} \int_0^T v_{F-F}(\theta) d\theta = \frac{3}{\pi} \int_{\frac{\pi}{3}}^{\frac{2\pi}{3}} \sqrt{2}V_{RnSn} \sin(\theta) d\theta \quad (13)$$

The integral of the DC input medium voltage is:

$$V_{CC} = \frac{3}{\pi} \int_{\frac{\pi}{3}}^{\frac{2\pi}{3}} 0.8794\sqrt{2}\sqrt{3}V_A \sin(\theta) d\theta = 2.0570V_A \quad (14)$$

$$V_A = \frac{V_{CC}}{2.0570} \quad (15)$$

B. Autotransformer Analysis

3) *RMS current in the windings* - For the mathematical analysis, currents in the windings and the injected current were decomposed at the Fourier series.

$$i_{An}(\omega t^\circ) = \sum_{k=1,3,5,\dots}^{\infty} \frac{4I_{CC}}{k\pi} \cos\left(\frac{k\pi}{6}\right) \sin\left(\frac{k\pi}{180^\circ} \omega t^\circ\right) \quad (16)$$

$$i_{LA}(\omega t^\circ) = \sum_{k=1,3,5,\dots}^{\infty} \left\{ \left[\frac{2}{N_{20^\circ}} \cos\left(100^\circ \frac{k\pi}{180^\circ}\right) - \frac{1}{N_{0^\circ}} \right] \frac{4I_{CC}}{k\pi} \cos\left(\frac{k\pi}{6}\right) \sin\left(\frac{k\pi}{180^\circ} \omega t^\circ\right) \right\} \quad (17)$$

$$i_A(\omega t^\circ) = \sum_{k=1,3,5,\dots}^{\infty} \left\{ \left[\frac{2}{N_{20^\circ}} \cos\left(100^\circ \frac{k\pi}{180^\circ}\right) + 2 \cos\left(20^\circ \frac{k\pi}{180^\circ}\right) - \frac{1}{N_{0^\circ}} + 1 \right] \frac{4I_{CC}}{k\pi} \cos\left(\frac{k\pi}{6}\right) \sin\left(\frac{k\pi}{180^\circ} \omega t^\circ\right) \right\} \quad (18)$$

Thus, the current at the secondary windings is given by:

$$I_{An} = \sqrt{\sum_{k=1,3,5,\dots}^{\infty} \left[\frac{4I_{CC}}{2k\pi} \cos\left(\frac{k\pi}{6}\right) \right]^2} = 0.8614I_{CC} \quad (19)$$

Analogously, the values of the currents at the primary windings and the grid current are:

$$I_{LA} = 0.2347I_{CC} \quad (20)$$

$$I_A = 2.0673I_{CC} \quad (21)$$

C. Apparent Power processed by the autotransformer

1) *Secondary windings* - The apparent power at the windings is obtained from the multiplication of the voltage of the winding by the current which passes across it.

$$S_{A1} = V_{A1}I_{A1} = \frac{V_A}{N_{20^\circ}} 0.8614I_{CC} = 0.2835V_A I_{CC} \quad (22)$$

The apparent power at the phased windings is given by:

$$S_{An} = V_{An}I_{An} = \frac{V_A}{N_{0^\circ}} 0.8164I_{CC} = 0.0985V_A I_{CC} \quad (23)$$

The total apparent power of the secondary is composed by the amount of power of every winding; The transformer has 6 windings shifted by 20° and 3 windings in phase, therefore:

$$S_S = 6S_{20^\circ} + 3S_{0^\circ} = 1.9965V_A I_{CC} = 1.9965 \frac{V_{CC}}{2.0570} I_{CC} \quad (24)$$

$$S_S = 0.9706V_{CC} I_{CC} \quad (25)$$

2) *Primary windings* - The total apparent power at the primary is the addition of the power at the 3 primary windings:

$$S_P = 3 \cdot 0.2347V_A I_{CC} = 0.7041 \frac{V_{CC}}{2.0570} I_{CC} \quad (26)$$

$$S_P = 0.3423V_{CC} I_{CC} \quad (27)$$

D. Total Power processed by the autotransformer

The total apparent power of the transformer is given by the average of the primary and secondary total power:

$$S_T = \frac{0.3423V_{CC} I_{CC} + 0.9706V_{CC} I_{CC}}{2} = 0.6564V_{CC} I_{CC} \quad (28)$$

The total average power provided by the inverters is the amount of the power provided by each inverter. Therefore:

$$P_{CC} = 3V_{CC} I_{CC} \quad (29)$$

The total apparent power of the transformer as function of the power provided by the inverters is given by:

$$S_T = 0.6564 \frac{P_{CC}}{3} = 0.2188P_{CC} \quad (30)$$

Thus, it is possible to verify that the total power processed by the transformer is 21.88% of the power provided by the inverters.

E. Harmonic content analysis of the autotransformer's current

1) *Entrance current harmonic distortion rate* - The harmonical distortion rate is given by the following expression:

$$THD\% = \frac{\sqrt{I_{RMS}^2 - I_1^2}}{I_1} = 10.05\% \quad (31)$$

Where I_1 is the value of the fundamental component. As the displacement factor is null, the power factor relation is presented such as follow:

$$FP = \frac{1}{\sqrt{1+THD^2}} = 0.9949 \quad (32)$$

The relations above shows this structure presents a high power factor and low THD.

V - DESIGN EXAMPLE

To validate the mathematical analysis, a prototype of the inverter was built according to specifications shown at TABLE II.

TABLE II
Grid inverter Specifications

| | |
|--|---------|
| RMS Grid Voltage (V_A) | 220 V |
| Grid frequency (f_{rede}) | 60 Hz |
| Number of photovoltaic panels | 18 |
| Peak power of each panel | 130 W |
| Peak power supplied to the overall system (P_{CC}) | 2340 W |
| Panels voltage (V_{CC}) | 261.2 V |
| Current supplied to each inverter (I_{CC}) | 2.985 A |

The physical design of the autotransformer was based on [4]. The number of turns of the primary windings is obtained by the Faraday's law and the secondary windings use the transformation relations. The method presented in [4] defines the product of the area of the central leg of the core window area. K_f , K_u e K_j factors are, respectively, form factors ($K_f = 4$ for the square wave), utilization factor ($K_u = 0.4$) and temperature rise ($K_j = 304$ for 25°C of temperature rise). The magnetic field of a silicon iron core can regard 1.1 T.

$$A_p = \left(\frac{S_T \cdot 10^4}{K_f K_m f_{rede} K_u K_j} \right)^{1.14} = \left[\frac{511.99 \cdot 10^4}{4 \cdot 1.1 \cdot 60 \cdot 0.4 \cdot 304} \right]^{1.14} = 356.8 \text{ cm}^4 \quad (33)$$

For constructive reasons, the chosen values for A_j and A_c were 500cm^4 and 12.34cm^2 respectively.

The number of turns is given by (34):

$$N_A = \frac{V_{LA} \cdot 10^4}{K_f B_m A_c f_{rede}} = \frac{127 \cdot 10^4}{4 \cdot 1.1 \cdot 12.35 \cdot 60} = 390 \text{ turns} \quad (34)$$

The currents and voltages in the autotransformer windings are shown at TABLE III.

TABLE III
Currents and voltages in the autotransformer windings

| Windings | RMS Voltage | RMS Current | Wire | Turns |
|---|-------------|-------------|--------|-------|
| N_{LA}, N_{LB}, N_{LC} | 127 V | 0.701 A | AWG 23 | 390 |
| $N_{A1}, N_{B1}, N_{C1},$ N_{A2}, N_{B2}, N_{C2} | 44.107 V | 2.438 A | AWG 18 | 136 |
| N_{An}, N_{Bn}, N_{Cn} | 15.318 V | 2.438 A | AWG 18 | 48 |

The built prototype is shown in Fig. 12.

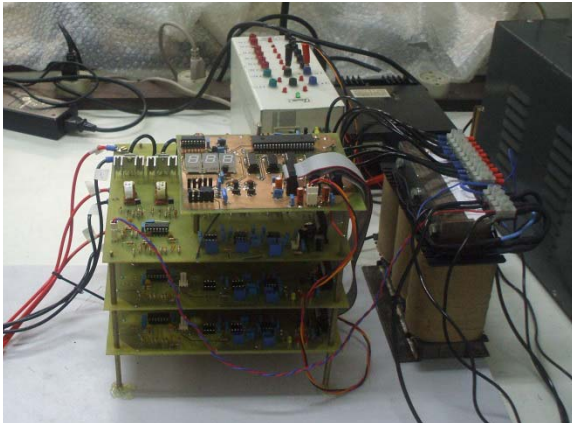


Fig. 12. Experimental Prototype

VI - EXPERIMENTAL RESULTS

A. Main Waveforms

This section presents the preliminary and complete experimental results of the implemented prototype. The preliminary results are composed without the use of a lowpass filter and the complete results are made with the using of it.

Fig. 13 shows the voltage at the primary windings of the transformer with the voltages of the subsystems, showing that the shift between them is approximately of 20° . This information can also be found at TABLE IV. A small variation appears due to non-idealities at the autotransformer windings.

TABLE IV
Discrepancy between subsystems 1, 2 and n

| | |
|-----|----------------|
| 1-2 | 41.68° |
| 1-n | 20.95° |
| 2-n | -20.73° |

Fig. 14 shows the inverter's input current and voltage at phase A. As can be seen, the input voltage has 6-pulse ripple as expected. The gate pulse angle is minor than 180° to allow the SCR turn-on with positive voltage across its terminals.

Fig. 15 shows current and voltage at the AC side of the inverter.

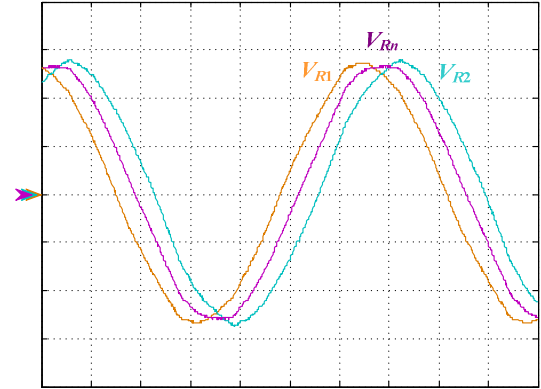


Fig. 13. Voltages on the primary and secondary of the autotransformer. (60V/div, 2.5ms/div)

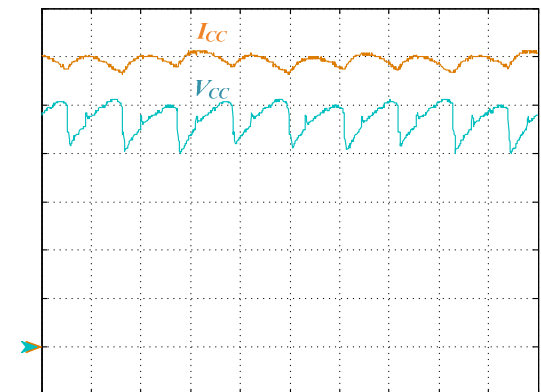


Fig. 14 – Input DC voltage and current at the inverters. (500mA/div, 60V/div, 2.5ms/div)

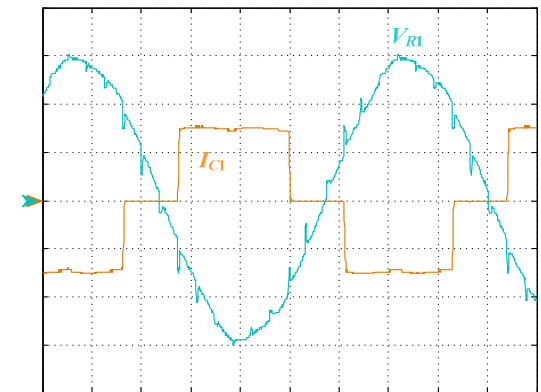


Fig. 15 – Voltage and current injected in the autotransformer by a phase A of phase-controlled inverter. (2A/div, 60V/div, 2.5ms/div)

Fig. 16 shows the voltage and current at the grid connection. As can be seen, the output current has an 18-pulse waveform, confirming the theoretical analysis. The current has a quasi-sinusoidal behavior and just needs a high frequency filter to comply with the IEEE-519-1992 standards.

Fig. 17 shows the three-phase currents injected in the grid.

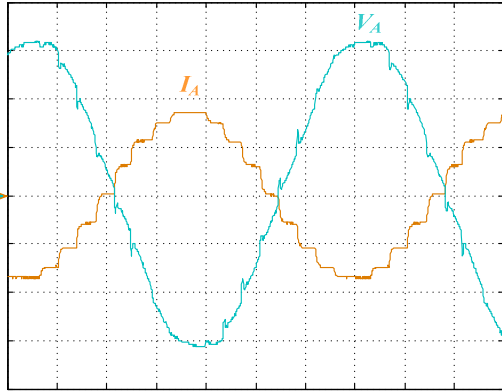


Fig. 16 – Output voltage and current injected at phase A of the grid. (5A/div, 60V/div, 2.5ms/div)

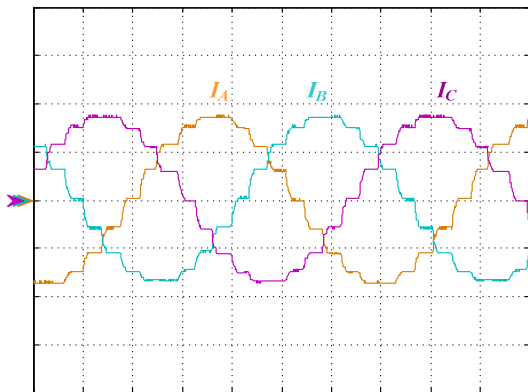


Fig. 17 – Currents injected in the grid. (5A/div, 2.5ms/div)

The following tables are composed by experimental results taken without the use of a lowpassfilter. TABLE V presents the power output specifications for each phase.

TABLE V
Power output specifications for each phase

| Phase | Power (P) | Reactive Power (Q) | Power Factor(f_p) | Phase Angle(\square) |
|-------|-----------|--------------------|-----------------------|--------------------------|
| A | -809W | 166VAR | -0.980 | 168.4° |
| B | -811W | 147VAR | -0.984 | 169.7° |
| C | -808W | 168VAR | -0.979 | 168.3° |

TABLE VI shows input specifications (voltage, current and power provided by the DC source) for phases A, B and C.

TABLE VI
Input specifications for each phase

| Phase | V_{CC} | I_{CC} | P_{CC} |
|-------|----------|----------|----------|
| A | 284V | 2.96A | 836W |
| B | 284V | 2.99A | 847W |
| C | 280V | 2.87A | 799W |

TABLE VII presents the projects's power specifications: the power provided by the DC source (P_{CC}) and the output power (P_{OUT}), along with the system's experimental efficiency:

TABLE VII
Project's power and efficiency specifications

| | |
|------------|--------|
| P_{CC} | 2482W |
| P_{OUT} | 2428W |
| Efficiency | 97.82% |

B. Harmonics

In this section it will be analyzed the harmonical contents injected into the grid. By the analysis of the experimental waveforms (without the use of a lowpass filter), not expectable harmonics were noticed. Theoretically, only harmonics of 17, 19, 35 and 37 orders were expected. But, due to non-idealities in the experimental tests, harmonics of 5, 9, 23 orders (among others) also appeared. Those extra harmonics appear due to the non-idealities of the grid voltages. The expected THD was 10%, but the experimental results pointed an 8.76% distortion.

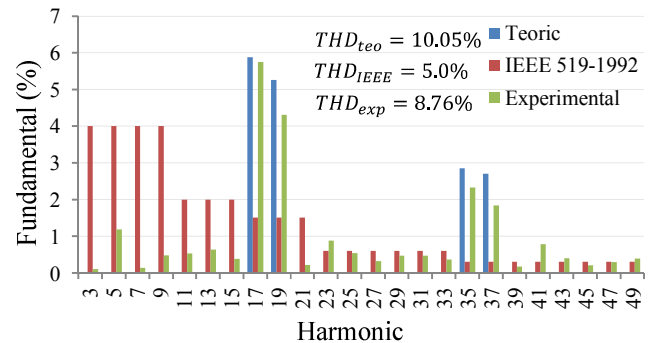


Fig. 18. Harmonic current injected in the grid

C. Low-pass filter

Even though, some harmonics have higher amplitudes than the required limits by norm. Aiming to meet these requirements, an output low pass filter was implemented in the converter.

The chosen filter was a LC low-pass filter, the capacitor is connected on the side of the autotransformer and the inductor is connected in the grid, as show at Fig. 19.

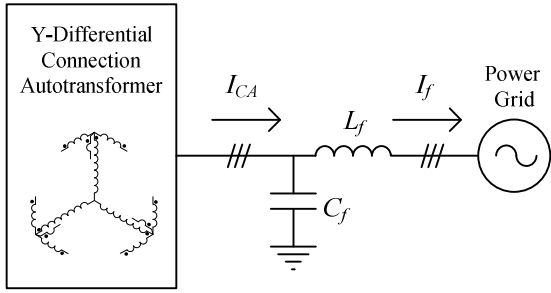


Fig. 19. Low pass filter connected to the converter

Fig. 20 shows the implemented LC filter.

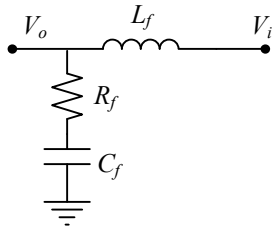


Fig. 20. LC filter

The transfer function of the filter is shown at (35). The resistor is used to reduce the resonant peak.

$$\frac{V_o}{V_i} = \frac{sR_f C_f + 1}{L_f C_f s^2 + sR_f C_f + 1} \quad (35)$$

The capacitor was selected according to the maximum reactive energy drained by the filter. The chosen value was about 10% of the nominal current. The inductor was defined by the cut frequency, as presented at (36).

$$f_c = \frac{1}{2\pi\sqrt{L_f C_f}} \quad (36)$$

The damping resistor is chosen aiming to attenuate the resonant peak: the higher the value, the lower the peak. Nevertheless, the impedance for high frequencies gets higher, damaging the filter's attenuation capacity.

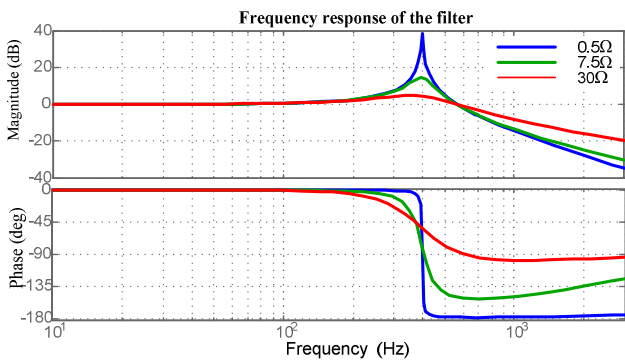


Fig. 21. Frequency response of LC filter with variations of damping resistor value

The filter parameters are shown at TABLE VIII.

TABLE VIII

Parameters of the implemented LC filter

| Parameter | Value |
|---------------|--------------|
| Cut frequency | 400 Hz |
| C_f | 10 μ F |
| L_f | 16 mH |
| R_f | 7.5 Ω |

The complete experimental results were taken using a lowpass filter, which contributed to the reduction of harmonic distortions to a 3.93% rate. The waveforms can be seen at Fig. 22 and Fig. 23.

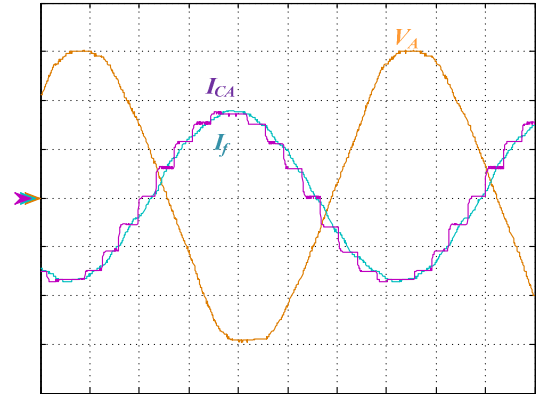


Fig. 22. Voltage of phase A and comparison between the current without the using of a filter (I_{CA}) and current with the filter (I_f). (60V/div, 5A/div, 2.5ms/div)

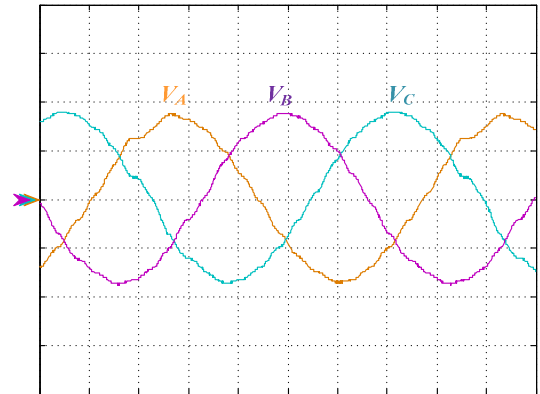


Fig. 23. Currents of phases A, B and C injected at the grid. (5A/div, 2.5ms/div)

Fig. 24 presents a comparison between currents injected in the grid before using a filter and after the utilization of it. It is possible to notice that all harmonical contents meet the legal standards and the THD has a rate of less than 5%.

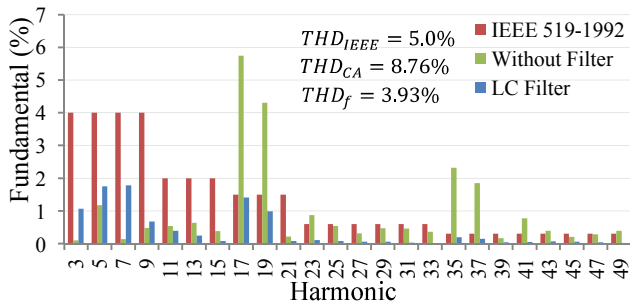


Fig. 24. Comparison of the harmonic contents (before and after the implementation of a LC filter) with norms required by IEEE 519-1992

VII - CONCLUSIONS

This paper presented a possible solution for the processing of photovoltaic energy, when the objective is presenting a low-cost and robust system to be installed mainly in remote locations.

The use of a phase-controlled inverter associated to an 18-pulse autotransformer guarantee a robust and cheaper option. The inverter technology is well dominated and uses silicon controlled rectifiers, which have a low cost compared to others switches (i.e. IGBTs used in commercial grid tie inverters). The 18-pulse autotransformer in fork configuration processes only 21.88% of the total power, reducing the overall cost and having a lot of robustness.

The complete experimental results confirm the system can work correctly and, with the utilization of a low-pass filter, it is possible to reduce the harmonics, meeting the IEEE 519-1992 standard.

Other noticeable characteristic is the high efficiency of this converter: 97.82% (experimentally obtained). This feature is important in photovoltaic applications and shows the converter meets the desirable standards.

The forward steps of this project proposes the elaboration of a MPPT algorithm using the variation of the thyristors shooting angle variation as a standard, changing the voltage of the panels, always aiming to obtain the maximum power.

VIII - REFERENCES

- [1] I. Barbi, *Eletrônica de Potência*, Editora da UFSC, 6th Edition, Florianópolis, Brazil, 1986.
- [2] F. J. M. Seixas, I. Barbi, "A New 12kW Three-Phase 18-Pulse High Power Factor AC-DC Converter With Regulated Output Voltage For Rectifier Units." in *International Telecommunications Energy Conference*, vol. 21, section 14-2, 1999.
- [3] P. S. Oliveira, R. C. Fernandes, F. J. M. Seixas, "Generalization of Wye and Delta Auto-Connections: Analysis of Voltages and Currents." in *International Conference on Industry Applications*, vol. 09, pp. 1-6, 2010.
- [4] C. Maclyman, *Transformer And Inductor Design Handbook*, Marcel Bekken And Basel, 3rd Edition New York, USA, 2004.
- [5] A. MARTIGNONI, *Transformadores*, Globo, 1st Edition, Porto Alegre, Brasil 1973.
- [6] F. J. M. Seixas, I. Barbi, "A New 18-Pulse AC-DC Converter With Regulated DC Output and High Power Factor for Three-Phase Applications" in *Proc. of COBEP*, vol. 05, 1999.
- [7] F. J. M. Seixas, I. Barbi, "A New Three-Phase Low THD Power Supply With High-Frequency Isolation And 60V/200A Regulated DC Output." in *Power Electronics Specialists Conference*, vol. 03, pp. 1629-1632, 2001.
- [8] F. J. M. Seixas, V. A. Gonçalves, "Generalization of the Delta-Differential Autotransformer for 12 and 18-Pulse Converters." in *IEEE Power Electronics Specialists Conference*, vol 36, pp. 460-466.